# Quantification of fossil fuel $CO_2$ from combined CO, $\delta^{13}CO_2$ and $\Delta^{14}CO_2$ observations

Jinsol Kim[1], John B. Miller[2], Charles E. Miller[3], Scott J. Lehman[4], Sylvia E. Michel[4], Vineet Yadav[3], Nick E. Rollins[1], and William M. Berelson[1]

[1]Department of Earth Sciences, University of Southern California, Los Angeles, CA 90089, USA
[2]Oceanic and Atmospheric Administration Global Monitoring Laboratory, Boulder, CO 80305, USA
[3]Jet Propulsion Laboratory, California Institute of Technology, Pasadena, CA 91109, USA
[4]Institute of Arctic and Alpine Research, University of Colorado, Boulder, CO 80309, USA

*Correspondence to*: Jinsol Kim (jinsolki@usc.edu)

**Abstract.** We present a new method for partitioning observed $CO_2$ enhancements ($CO_2$xs) into fossil and biospheric fractions ($C_{ff}$ and $C_{bio}$) based on measurements of CO and $\delta^{13}CO_2$, complemented by flask-based $\Delta^{14}CO_2$ measurements. This method additionally partitions the fossil fraction into natural gas and petroleum fractions (when coal combustion is insignificant). Although here we apply the method only to discrete flask air measurements, the advantage of this method (CO and $\delta^{13}CO_2$-based method) is that $CO_2$xs partitioning can be applied at high frequency when continuous measurements of CO and $\delta^{13}CO_2$ are available. High frequency partitioning of $CO_2$xs into $C_{ff}$ and $C_{bio}$ has already been demonstrated using continuous measurements of CO (CO-based method) and $\Delta^{14}CO_2$ measurements from flask air samples. We find that the uncertainty in $C_{ff}$ estimated from the CO and $\delta^{13}CO_2$-based method averages 3.2 ppm (23 % of the mean $C_{ff}$ of 14.2 ppm estimated directly from $\Delta^{14}CO_2$) which is significantly less than the CO-based method which has an average uncertainty of 4.8 ppm (34 % of the mean $C_{ff}$). Using measurements of CO, $\delta^{13}CO_2$ and $\Delta^{14}CO_2$ from flask air samples at three sites in the greater Los Angeles region, we find large contributions of biogenic sources that vary by season. On a monthly average, the biogenic signal accounts for $-14$ to $+25$ % of $CO_2$xs with larger and positive contributions in winter and smaller and negative contributions in summer due to net respiration and net photosynthesis, respectively. Partitioning $C_{ff}$ into petroleum and natural gas combustion fractions reveals that the largest contribution of natural gas combustion generally occurs in summer, which is likely related to increased electricity generation in LA power plants for air-conditioning.

# 1 Introduction

The world's cities account for up to 70 % of global greenhouse gas (GHG) emissions, while covering less than 2 % of the Earth's surface (IPCC, 2014). Cities around the world have started implementing mitigation strategies to reduce carbon dioxide ($CO_2$) emissions and collaborate with each other in organizations such as the C40 Cities Climate Leadership Group (https://www.c40.org/) and the Global Covenant of Mayors for Climate and Energy (https://www.globalcovenantofmayors.org/). To support urban efforts, monitoring systems are necessary to evaluate and verify reductions attributable to specific mitigation strategies (Turnbull et al. 2022).

Current understanding of anthropogenic $CO_2$ emissions mainly derives from methods that estimate aggregate emissions in a domain using economic statistics such as total fuel sales or activity data such as total distance traveled for on-road vehicle emissions. These "bottom-up" methods provide specific location and process information that rely on mapping the source-specific emission factors and measurements of activities (e.g., McDonald et al. 2014; Gurney et al. 2019; Gately and Hutyra 2017; Super et al. 2020). In contrast, more recently "top-down" methods that quantify emissions from measurements of atmospheric $CO_2$ have been used to estimate emissions. These top-down approaches typically use either a mass balance technique where an initial estimate is not required (e.g. Mays et al. 2009; Cambaliza et al. 2014; Heimburger et al. 2017; Ahn et al. 2020) or an inverse/data assimilation approach where observations and a prior map of emissions are combined to generate a best estimate (e.g. Bréon et al. 2015; Staufer et al. 2016; Sargents et al. 2018; Turner et al. 2020; Lauvaux et al. 2016, 2020).

To estimate anthropogenic $CO_2$ emissions using top-down method, it is crucial to separate the fossil fuel signals from the biogenic signals, which can vary from negative (uptake) to positive (emission) across the annual cycle. Recent analyses of urban $CO_2$ suggest that biogenic emissions and uptake have significant magnitudes relative to fossil fuel fluxes, especially during the growing season (Sargent et al., 2018; Vogel et al., 2019; Miller et al., 2020). Previous top-down studies used biosphere models to estimate biogenic fluxes and then focused on determining the balance of emissions attributable to fossil fuel combustion assuming that the biogenic emissions are known (Sargent et al. 2018; Turner et al. 2020; Lauvaux et al. 2020). However, even with recent improvements in biosphere models (Wu et al. 2021; Gourdji et al. 2022) the actual magnitude and variability of these fluxes are still not well constrained (Hardiman et al., 2017; Winbourne et al.,

2022), potentially leading to unknown observational bias in the associated estimates of fossil fuel derived emissions.

Radiocarbon ($^{14}CO_2$) provides the ability to separate biogenic and anthropogenic $CO_2$ fluxes and mole fractions from an observational point of view (e.g. Levin, 2003; Turnbull 2006). Observational methods rely on the fact that fossil fuels and the resultant $CO_2$ produced during combustion are completely devoid of $^{14}C$ (i.e., $\Delta^{14}C_{ff}$ = -1000‰ on the widely used Delta scale; Stuiver and Polach, 1977). Measurements of $\Delta^{14}CO_2$, acquired at time scales of weeks to months, allow quantification of seasonal variations in biogenic and fossil contributions to the atmospheric $CO_2$ mole fraction (e.g., Djuricin et al. 2010; Miller et al. 2012; Turnbull et al. 2015). $^{14}C$ methods typically require air sample collection, preparation and analysis via accelerator mass spectrometry which limits the number of measurements, although a number of promising optical methods for in situ $^{14}CO_2$ measurement at natural abundance are currently being developed (Fleisher et al. 2017; Genoud et al. 2019; McCartt and Jiang 2022).

On the other hand, carbon monoxide (CO) is a widely used tracer that can be measured continuously in situ using high-precision optical analyzers (e.g. Vogel et al. 2010; Newman et al. 2013; Turnbull et al. 2015; Lauvaux et al. 2020). CO is often co-emitted with fossil fuel $CO_2$ ($CO_2$ff) during incomplete combustion. If the $COxs:CO_2ff$ ratio ($R_{ff}$, where $COxs$ is the CO enhancement above background) is well constrained, continuous CO measurements combined with $R_{ff}$ can provide an estimate of continuous $CO_2$ff. A few studies have applied this method to estimate fossil fuel emissions for a moment in time during an airborne measurement campaign (Graven et al. 2009; Turnbull et al. 2011). However, this approach is challenging to identify interannual trends because $R_{ff}$ at a site may vary significantly on timescales ranging from hours to years (Levin and Karstens, 2007; Vogel et al., 2010). $CO:CO_2$ emission ratio can vary by sources depending on the carbon content of the fuel and combustion conditions. Due to the impacts of atmospheric transport at a given observation site and the variability in the source combination in time and space, $R_{ff}$ also varies in time and space. Additionally, CO produced from oxidation of volatile organic compounds (VOCs) can have an effect (Vimont et al., 2019).

Vardag et al. (2015) proposed dividing fossil fuel emissions further into two groups that may display less variability in $CO:CO_2$ emission ratio. If one group is well constrained by CO and the other by $^{13}CO_2$, each group can be identified by combining CO and $^{13}CO_2$ observations. Vardag et al. focused on separating traffic from non-traffic emissions, or biofuel emissions from the other

fossil fuel emissions. However, no significant benefit of combining CO and $^{13}CO_2$ was found because traffic and biofuel $CO_2$ do not produce distinct $CO:CO_2$ emission ratio or $^{13}CO_2$ isotopic signatures compared to the other $CO_2ff$ source terms.

Here, we differentiate $CO_2$ signals from biogenic, petroleum and natural gas sources by combining CO, $\delta^{13}CO_2$, and $\Delta^{14}CO_2$ measurements. The combination of $\Delta^{14}CO_2$ and $\delta^{13}CO_2$ has been used previously to distinguish biogenic, petroleum and natural gas signals for air sampling events (Lopez et al. 2013; Djuricin et al. 2010) and at seasonal scale (Newman et al., 2016). In contrast, the combination of CO and $\delta^{13}CO_2$, which can both be measured at high frequency, enables source partitioning at higher temporal resolution. We demonstrate the agreement between the existing $\Delta^{14}CO_2$, $\delta^{13}CO_2$ and newly proposed CO, $\delta^{13}CO_2$ methods. This establishes the utility of the CO and $\delta^{13}CO_2$ in partitioning $CO_2xs$ into fossil fuel and biogenic components, with further partitioning of fossil fuel sources into petroleum and natural gas sources, in the Los Angeles megacity.

## 2 Methods

Here, we describe two methods for separating fossil fuel and biogenic components from atmospheric $CO_2$ measurements in the complex urban environment of the Los Angeles megacity (LA). Section 2.2 describes our application of the method already described by Newman et al. (2016) using $\Delta^{14}CO_2$ and $\delta^{13}CO_2$ observations. The details of the new method utilizing CO and $\delta^{13}CO_2$ measurements are described in section 2.3. Briefly, we take advantage of the fact that the combination of the $CO:CO_2$ emission ratio and the $^{13}CO_2$ isotopic signature reveal a very distinct pattern for biogenic, petroleum and natural gas sources. However, this approach requires knowledge of the $CO:CO_2$ emission ratio and the isotopic signature of each source. We apply isotopic signatures reported by previous studies, and $CO:CO_2$ emission ratios are determined for LA using measurements of CO, $\delta^{13}CO_2$ and $\Delta^{14}CO_2$ from flask samples. Flask measurements are described in section 2.1 and the source apportionment from $\Delta^{14}CO_2$ and $\delta^{13}CO_2$ observations, which is used to derive $CO:CO_2$ emission ratios for each source, is described in section 2.2.

### 2.1 Measurements

120  We use measurements from air samples collected at 2 p.m. local standard time at three existing Los Angeles Megacity Carbon Project sites: University of Southern California (USC), California State University, Fullerton (FUL), and Granada Hills (GRA) (Miller et al., 2020). Air samples were collected from November 2014 to March 2016 using National Oceanic and Atmospheric Administration (NOAA) programmable flask packages (PFPs) and programmable compressor

125  packages (Sweeney et al., 2015). The samples were sent back to the NOAA Global Monitoring Laboratory where greenhouse gases including $CO_2$ as well as CO mole fractions were measured using NOAA's high-precision/high-accuracy greenhouse gas measurement system (Sweeney et al., 2015). After the measurement, residual air is extracted from PFP flasks and $CO_2$ is isolated for $^{14}C$ measurement using established cryogenic and mass spectrometric techniques (Lehman et al., 2013).

130  Samples are purified, graphitized and packed into individual targets at the University of Colorado, Boulder, Institute of Arctic and Alpine Research (INSTAAR) and then sent to the University of California, Irvine, Keck Accelerator Mass Spectrometry Facility for high- precision $\Delta^{14}C$ measurement. One-sigma measurement uncertainty is $\sim 1.8$ ‰, equivalent to $\sim 1.2$ parts per million (ppm) of recently added fossil fuel–$CO_2$. $\delta^{13}CO_2$ in PFP samples is measured by dual inlet

135  isotope ratio mass spectrometry with a precision of approximately 0.02 ‰ at the INSTAAR Stable Isotope Laboratory (Vaughn et al., 2004; Sweeney et al., 2015)

Enhancement of each species is defined relative to a time-dependent background level, which is based on nighttime (2 AM local standard time) measurements made at Mount Wilson Observatory (MWO; Fig. 1) located at 1,670 m above sea level. Nighttime air at MWO generally represents the

140  relatively clean, well-mixed free troposphere since polluted LA Basin boundary layer air has typically descended back into the basin by this time. After an additional step of filtering obvious outliers corresponding to pollution events indicated by anomalously elevated values were interpolated to the time of observations within the LA Basin by fitting curves to the screened MWO data (Fig. 2). A further analysis of associated CO measurements indicates that background

145  reconstructed using nighttime air samples from MWO is representative of clean background air coming from either on- or off-shore (Miller et al., 2020).

**2.2 Partitioning $CO_2$ signals using flask-based $\Delta^{14}CO_2$ and $\delta^{13}CO_2$ measurements**

Our general approach to distinguishing $CO_2$ signals from biogenic, petroleum and natural gas sources using $\Delta^{14}CO_2$ and $\delta^{13}CO_2$ follows the procedure described by Newman et al. (2016). Following previous derivations (e.g., Turnbull et al, 2006; Miller et al. 2020), we start with the definition for $CO_2ff$ which is based on mass balances for the atmospherically conserved quantities $\Delta^{14}C \times CO_2$ and $CO_2$:

$$C_{ff} = \frac{C_{obs}(\Delta_{obs}-\Delta_{bkg})}{(\Delta_{ff}-\Delta_{bkg})} - \frac{C_r(\Delta_r-\Delta_{bkg})}{(\Delta_{ff}-\Delta_{bkg})} \qquad (1)$$

Measured $CO_2$ mole fractions and $\Delta^{14}C$ values are abbreviated as $C$ and $\Delta$. Subscripts 'obs', 'bkg', 'ff' and 'r' represent observations, background, fossil fuel, and respiration, respectively. $\Delta_{ff}$ is equal to $-1000$ ‰. As in the Miller et al. (2020) study focusing on LA, we estimate the value of the small respiratory term, $C_r(\Delta_r - \Delta_{bkg})/(\Delta_{ff} - \Delta_{bkg})$, as 0.25 ppm. The overall uncertainty of $C_{ff}$ for LA measurements during 2015 is approximately 1.2 ppm, which includes 100% uncertainty assigned to the respiratory term. $C_{ff}$ and $C_{bio}$ ($C_{bio} = C_{xs} - C_{ff}$) are calculated for all available flask air samples during the 2014 – 2016 sampling period, a frequency of approximately three times per week at each of the three sites.

$C_{ff}$ is then separated into signals from petroleum and natural gas combustion using $^{13}C:^{12}C$ ratios ($\delta^{13}C$ as defined by standard isotopic definition; Craig, 1957) measured on the same air samples. First, the flux weighted-mean $\delta^{13}C$ signature of all sources located in the observation footprints ($\delta_{src}$) is determined on a sample-by-sample basis using the combined mass balances for $\delta^{13}C \times CO_2$ and $CO_2$:

$$\delta_{src} = \frac{\delta_{obs} \times C_{obs} - \delta_{bkg} \times C_{bkg}}{C_{obs} - C_{bkg}} \qquad (2)$$

where $\delta$ is short-hand for $\delta^{13}CO_2$. The uncertainties in $C_{obs}$, $C_{bkg}$, $\delta_{obs}$, and $\delta_{bkg}$ are 0.1 ppm, 1.5 ppm, 0.02 ‰, and 0.08 ‰, respectively. The "obs" uncertainties are measurement uncertainties, while the "bkg" uncertainties are determined as the standard deviation of the difference between the observations and their smoothed curve representation at MWO. The median uncertainty in $\delta_{src}$ is 3.0 ‰ and is calculated by propagating the uncertainties listed above, including covariance between $\delta^{13}C$ and $\delta^{13}C \times CO_2$.

We combine $C_{ff}$ (eq. 1) and $\delta_{src}$ (eq. 2) to determine the $\delta^{13}C$ signature of fossil fuel emissions, $\delta_{ff}$:

$$\delta_{src} = \delta_{ff} \times f_{ff} + \delta_{bio} \times (1 - f_{ff}) \tag{3}$$

Rearranging yields:

$$\delta_{ff} = \frac{\delta_{src} - \delta_{bio} \times (1 - f_{ff})}{f_{ff}} \tag{4}$$

where $f$ is the fraction. Following Newman et al. (2016), we take the isotopic signature of biospheric $CO_2$ fluxes ($\delta_{bio}$) to be $-26.6 \pm 0.5$ ‰ based on the analysis of Northern Hemisphere mid-latitude $CO_2$ and $\delta^{13}C$ observations (Bakwin et al., 1998b), which reflects the predominance of $C_3$ photosynthesis. However, because LA turfgrasses, which could account for a significant fraction of urban $CO_2$ fluxes [Miller, 2020], are often $C_4$ species (e.g., Bermuda and Buffalo grasses), we also conduct tests using $\delta_{bio} = -20$ ‰, representing a C3/C4 mix (Fig. S1). When we change $\delta_{bio}$ from $-26.6$ ‰ to $-20$ ‰, $f_{pet}$ decreases by 0.04 and $f_{ng}$ increases by 0.05 which is smaller than the median uncertainty in $f_{pet}$ and $f_{ng}$ which is 0.17 and 0.16, respectively. $f_{ff}$ is the fraction of $C_{ff}$ in $C_{xs}$, i.e., $C_{ff}/C_{xs}$, and $1 - f_{ff} = f_{bio}$. Lastly, the proportion of $C_{ff}$ emitted by petroleum (pet) and natural gas (ng) combustion, $f_{pet}$ and $f_{ng}$, are calculated from the values of $\delta_{ff}$:

$$\delta_{ff} = \delta_{pet} \times f_{pet/ff} + \delta_{ng} \times (1 - f_{pet/ff}) \tag{5}$$

$$f_{pet/ff} = \frac{\delta_{ff} - \delta_{ng}}{\delta_{pet} - \delta_{ng}} \tag{6}$$

We use values of $-25.5 \pm 0.5$ ‰ for $\delta_{pet}$ (Newman et al. 2016; measurements in 2014) and $-40.2 \pm 0.5$ ‰ for $\delta_{ng}$ (Newman et al., 2008); $f_{pet} = f_{ff} \times f_{pet/ff}$, and $f_{ng} = f_{ff} \times f_{ng/ff}$, where $f_{ng/ff} = 1 - f_{pet/ff}$. We use temporally constant $\delta^{13}C$ signatures for petroleum, natural gas and biogenic sources (and sinks), although with additional processed-based information, this assumption could be relaxed in the future. Note that although pet, ng, and bio signatures are fixed, both $\delta_{src}$ and $\delta_{ff}$ vary with time, meaning that $f_{bio}$, $f_{pet}$ and $f_{ng}$ all vary at the frequency of the air sampling. Samples with calculated $f_{pet/ff}$ values outside the range of 0 and 1, corresponding to small $CO_2$xs and large uncertainty in $\delta_{src}$, are excluded from the analysis.

**2.3 Partitioning $CO_2$ signals using CO and $\delta^{13}CO_2$ measurements**

Although we can determine $f_{bio}$, $f_{pet}$ and $f_{ng}$ at the frequency of discrete flask sampling events using the method described in Section 2.2, here we describe how comparable $CO_2xs$ fractions can in theory be determined at high frequency using continuous measurements of CO and $\delta^{13}CO_2$. To evaluate the method, we compute the relative contributions of biogenic, petroleum and natural gas sources to $CO_2xs$ using flask air CO and $\delta^{13}CO_2$ measurements and compare these to values obtained using the $\Delta^{14}CO_2$-guided approach for the same samples by applying the following system of equations:

$$R_{src} = R_{bio} \times f_{bio} + R_{pet} \times f_{pet} + R_{ng} \times f_{ng} \tag{7}$$

$$\delta_{src} = \delta_{bio} \times f_{bio} + \delta_{pet} \times f_{pet} + \delta_{ng} \times f_{ng} \tag{8}$$

$$1 = f_{bio} + f_{pet} + f_{ng} \tag{9}$$

$R_{src}$ represents the $CO/CO_2$ ratio of the total source, which is the observed $COxs/CO_2xs$ ratio, and we use $R$ to refer to the $CO/CO_2$ emission ratios of individual $CO_2xs$ components (bio, pet, and ng). For now, we assume that $R$ of each source are constant over a year-long period and over the greater LA region (discussed in Section 3.2); especially with high frequency CO and $\delta^{13}CO_2$ measurements, this assumption could easily be relaxed (discussed in Section 3.3).

$R$ values and $\delta^{13}C$ signatures for bio, pet, and ng are needed to solve Eqs. 7-9. $\delta^{13}C$ signatures are specified in section 2.2; $R$ values are obtained via multiple linear regression of Eq. 7 using observed $R_{src}$ and $f$ values determined using $\Delta^{14}C$ and $\delta^{13}C$ of $CO_2$ measurements as described in Section 2.2. Then we solve Eqs. 7-9 for new $f$ values, $f'$. This new $CO_2xs$ partitioning (i.e., $f'_{bio}$, $f'_{pet}$, $f'_{ng}$) based on CO and $\delta^{13}CO_2$ observations is used to calculate new values of $C_{ff}$ and $C_{bio}$ (i.e., $C'_{ff}$ and $C'_{bio}$).

## 3   Results and Discussion

### 3.1 Contribution of biogenic, petroleum and natural gas sources in $CO_2$ excess

We calculated the fractional contribution of petroleum, natural gas, and biospheric fluxes to total $CO_2xs$ each month from April 2015 to March 2016 using $\Delta^{14}CO_2$ and $\delta^{13}CO_2$ observations recorded at FUL, USC and GRA. The results are given in Table S1 and presented in Figure 3. Figure 4 presents the results in terms of the relative $CO_2xs$ contribution from each source at each

site. We observe seasonal variation in $CO_2$xs from each source. Fossil fuel is the dominant $CO_2$ emissions source at each site which agrees with the findings of Newman et al. (2016) and Miller et al. (2020). Annually averaged across all three sites, biogenic emissions account for 6 % of $CO_2$xs. Biogenic emissions are larger and positive in winter and smaller and negative in summer, indicating winter respiration and uptake in summertime, generally consistent with the results of Miller et al. (2020). Note that in this study, we do not partition $C_{bio}$ into an urban biosphere component and other components related to the oxidation of biogenic carbon including ethanol added to gasoline, and human and other animal food and waste (which can only be positive and are unlikely to vary much seasonally). If, as in Miller et al. (2020), we accounted for the always positive ethanol, food, and waste signals, we would likely observe similarly large seasonal drawdown associated with urban vegetation.

We also observe spatial differences: The USC site exhibits a smaller contribution of the biosphere (3 % of annual average $CO_2$ excess) compared to FUL and GRA (9 % and 5 % of total $CO_2$ excess, respectively). However, these modest annual average biospheric contributions mask significant seasonal activity. On a monthly basis, maximum positive biogenic contribution is observed in November at 25 %, 26 %, and 22 % at USC, FUL, and GRA (percentage of total $CO_2$ excess, respectively). And the maximum negative contribution, driven by net photosynthesis, is observed in July with values of -22 %, -13 %, and -12 % at USC, FUL, and GRA (percentage of total $CO_2$ excess, respectively).

Network average $C_{ff}$ is 11.0 ± 14.5 ppm in winter (November-February; median and standard deviation) and 12.2 ± 6.6 ppm in summer (May-August). No significant difference is observed in winter and summer $C_{ff}$. This corresponds to the seasonality in Hestia-LA emissions, which indicates $C_{ff}$ inputs are only 3 % higher in winter. High variability observed in wintertime $C_{ff}$ agrees with Miller et al. (2020) which is likely caused by increased temperature inversion trapping as the cold ground surface in winter cools the air layer right above the ground. While Hestia-LA estimated relative contribution of petroleum and natural gas to fossil fuel emissions as 75 % and 25 %, we observe lower contribution of petroleum, 67 %, and larger contribution of natural gas, 33 %. Furthermore, the top-down seasonality of petroleum and natural gas (Fig. 4), which as fractions of $C_{ff}$ should be largely independent of mixing, are clearly evident. The proportion of natural gas in fossil fuel signals are 40 % and 36 % in summer and 34 % and 30% in winter at FUL and USC (Fig. 3). The increase in the natural gas contribution observed in summer can be

explained by the increase in natural gas generated electricity in LA power plants to provide for air

260    conditioning in summer (Newman et al., 2016; He et al., 2019). GRA, located northwest of USC by ~35 km without an electricity generation facility nearby, shows the opposite pattern (24 % in summer and 40 % in winter). This suggests the local influence of increased natural gas usage for heating in the winter.

**3.2 CO:CO₂ emission ratio ($R$) values of biogenic, petroleum and natural gas sources**

265    Monthly, site-based $R_{src}$ varies between $5.5 - 11.4$ ppb ppm$^{-1}$ (Fig. 5), with a mean and standard deviation of $8.2 \pm 1.6$ ppb/ppm (relative s.d. = 19 %). Greater variability is seen in $R_{ff}$ (lower panel): mean and s.d. of $9.6 \pm 2.1$ ppm (relative s.d. = 22 %). To understand and predict the variation in $R_{ff}$, we further divide the fossil fuel emissions into petroleum and natural gas emissions. Applying the calculated $f$ values from $\Delta^{14}CO_2$ and $\delta^{13}CO_2$ observations (Section 2.2.,

270    Fig. 3), we solve Eq. 7 for each source's CO/CO₂ emission ratio, $R$ (Table 2). Note that we exclude negative flask-based values of COxs (and corresponding $R_{src}$ values) and CO₂ff (and corresponding $f_{ff}$ values) as non-physical. Likewise, positive $\delta_{src}$ values and $f_{pet/ff}$ values (and corresponding $f_{pet}$ and $f_{ng}$ values) outside the range of 0-1 are also excluded. A bootstrapping method is used to calculate the mean and uncertainty of possible CO/CO₂ ratios. The CO/CO₂

275    ratios of petroleum ($R_{pet}$) and natural gas ($R_{ng}$) combustion emissions are $12.2 \pm 0.6$ ppb ppm$^{-1}$ and $2.3 \pm 1.2$ ppb ppm$^{-1}$, respectively. As discussed above, the proportion of natural gas in fossil fuel emissions is bigger in summer resulting in smaller $R_{ff}$ in summer at FUL and USC. We find the value of $1.8 \pm 0.8$ ppb ppm$^{-1}$ for $R_{bio}$ which is non-zero because biofuel (mainly corn-based ethanol) in the gasoline in California with large CO/CO₂ ratio signal is included in the biogenic

280    sources while respiratory CO/CO₂ ratios approach 0. A larger contribution of the biosphere with a low CO/CO₂ ratio in winter offsets the large $R_{ff}$ lowering the variability in $R_{src}$ at each site.

We compare our model-determined CO/CO₂ ratios of each source (Table 2) to bottom-up inventory-based estimates (Table 1). CO/CO₂ ratios of each source constrained from our model and observational data approach agree well with the bottom-up inventory-based estimates. Sources

285    contributing a high percentage of CO₂ emissions strongly influence the total CO/CO₂ ratio. The CO/CO₂ ratio of petroleum combustion is greatly affected by on-road emissions and industrial emissions (contributing 60 % and 28 % of total petroleum CO₂ emissions). Natural gas is mostly

dominated by non-mobile emissions (Electricity production, residential, commercial, and industrial, sequentially) resulting in low $CO/CO_2$ ratio.

## 3.3 Estimation of $CO_2ff$ based on CO and $^{13}CO_2$ observations

Table 2 shows the $CO/CO_2$ ratio and $\delta^{13}C$ signature of each source. The combination of the $R$ and $\delta$ signals reveal a distinct pattern for each source: the biosphere has low near-zero $R$, petroleum has high $R$, and natural gas has low $R$. Petroleum and biosphere $CO_2$ have similar $\delta$ values, whereas natural gas has a very low $\delta$. By substituting these values into Eqs. 7-9, $f'$ values are calculated, and then we calculate $C'_{ff}$ by multiplying the sum of $f'_{pet}$ and $f'_{ng}$ by $CO_2xs$ measured every few days. We compare $f'_{ff}$ and $C'_{ff}$ to $f_{ff}$ and $C_{ff}$ (determined using $^{14}C$ observations) in Fig. 6. Assessment for each source is shown in Figure S2 and S3. The $R^2$ values are 0.63 and 0.90 for $f'_{ff}$ and $C'_{ff}$, respectively.

If $R$ values are allowed to vary in time, it is likely to improve the precision of the method. We calculate the uncertainty in $C'_{ff}$ for varying temporal resolutions of $R$ (black solid line in Fig. 7). We find that the uncertainty increases when the size of the window increases from 1-week to 10-week; in other words, allowing temporal variation in $R$ improves the precision of the method. However, the uncertainty slightly decreases beyond the 10-week window. This is likely caused by the reduction in the error of $R$ values (not shown) as the number of observations used to find $R$ (by solving Eq. 7) increases. In summary, the ideal flask sampling frequency for this method would be higher than every 2 weeks. In cases where this is impossible, it is better to assume constant $R$ values.

The uncertainty in $C'_{ff}$ estimated using the CO-based method is also shown in Figure 7 (black dashed line). The CO-based method also provides improved precision of the method when flask sampling is available at higher frequency. However, the CO and $\delta^{13}CO_2$-based method shows greater confidence than the CO-based method for the whole range of adjusted temporal resolution in $R$. When using constant $R$ values (temporal resolution of 50 weeks), the uncertainty is 3.2 ppm (the $1\sigma$ standard deviation of differences between $C_{ff}$ and $C'_{ff}$) for the CO and $\delta^{13}CO_2$-based method, while it is 4.8 ppm for CO-based method. This improvement is likely associated with the additional information provided by $\delta^{13}CO_2$ that constrains the effective $R_{ff}$ and further separates fossil fuel sources into sub-categories (petroleum and natural gas sources).

**4 Conclusions**

We present a CO and $\delta^{13}CO_2$-based method to estimate $CO_2ff$ which is based on flask-based $\Delta^{14}CO_2$ measurements. We have applied the method to measurements from flask samples collected in the LA basin, every few days in the afternoon for more than one year (2015-16). The proposed method was assessed by comparing it to a more traditional $\Delta^{14}CO_2$-based method. CO and $\delta^{13}CO_2$ approach can be applied to continuous measurements of $CO_2$, CO and $\delta^{13}CO_2$ which can provide $CO_2ff$ estimates at higher temporal resolution and with greater accuracy than previously applied CO-based methods.

We have analyzed three locations in the Los Angeles megacity, partitioning observed $CO_2$ enhancements ($CO_2xs$) into biogenic, petroleum and natural gas sources. We observed a substantial biogenic signal that varies from -14% to +25% of $CO_2xs$ over the course of the year, with positive contributions in winter and negative contributions in summer due to net respiration and net photosynthesis, respectively. Furthermore, partitioning $CO_2ff$ into petroleum and natural gas combustion fractions revealed that natural gas combustion has the largest contribution in summer, potentially due to an increase in electricity generation at LA power plants for air conditioning.

**Data availability.** The data that support the findings of this study are available from JBM (john.b.miller@noaa.gov) upon request.

**Author contributions.** JK designed and executed the study. JBM, SJL, and SEM provided the data. JK prepared the manuscript with contributions from all co-authors

**Competing interests.** The authors declare that they have no conflict of interest.

**References**

Ahn, D. Y., Hansford, J. R., Howe, S. T., Ren, X. R., Salawitch, R. J., Zeng, N., Cohen, M. D., Stunder, B., Salmon, O. E., Shepson, P. B., Gurney, K. R., Oda, T., Lopez-Coto, I., Whetstone, J., and Dickerson, R. R.: Fluxes of Atmospheric Greenhouse-Gases in Maryland (FLAGG-MD): Emissions of Carbon Dioxide in the Baltimore, MD-Washington, D.C. Area, J. Geophys. Res.

Atmos., 125, 1–23, https://doi.org/10.1029/2019JD032004, 2020.

Bakwin, P. S., Tans, P. P., Andres, J., and Conway, C. O.: Determination of the isotopic (13C/12C) discrimination of atmospheric, Global Biogeochem. Cycles, 12, 555–562, 1998a.

350    Bakwin, P. S., Tans, P. P., White, J. W. C., and Andres, R. J.: Determination of the isotopic (13C/12C) discrimination of terrestrial biology from a global network of observations, Global Biogeochem. Cycles, 12, https://doi.org/10.1029/98GB02265, 1998b.

Bréon, F. M., Broquet, G., Puygrenier, V., Chevallier, F., Ramonet, M., Dieudonné, E., Lopez, M., Cea-cnrs-uvsq, U. M. R., and Yvette, G.: An attempt at estimating Paris area CO2 emissions

355    from atmospheric concentration measurements, Atmos. Chem. Phys., 1707–1724, https://doi.org/10.5194/acp-15-1707-2015, 2015.

Cambaliza, M. O. L., Shepson, P. B., Caulton, D. R., Stirm, B., Samarov, D., Gurney, K. R., Turnbull, J. C., Davis, K. J., Possolo, A., Karion, A., Sweeney, C., Moser, B., Hendricks, A., Lauvaux, T., Mays, K., Whetstone, J., Huang, J., Razlivanov, I., Miles, N. L., and Richardson, S.

360    J.: Assessment of uncertainties of an aircraft-based mass balance approach for quantifying urban greenhouse gas emissions, Atmos. Chem. Phys., 14, 9029–9050, https://doi.org/10.5194/acp-14-9029-2014, 2014.

Craig, H.: Isotopic standards for carbon and oxygen and correction factors for mass-spectrometric analysis of carbon dioxide, Geochim. Cosmochim. Acta, 12,

365    https://doi.org/10.1016/0016-7037(57)90024-8, 1957.

Djuricin, S., Pataki, D. E., and Xu, X.: A comparison of tracer methods for quantifying CO2 sources in an urban region, J. Geophys. Res., 115, 1–13, https://doi.org/10.1029/2009JD012236, 2010.

Fleisher, A. J., Long, D. A., Liu, Q., Gameson, L., and Hodges, J. T.: Optical Measurement of

370    Radiocarbon below Unity Fraction Modern by Linear Absorption Spectroscopy, J. Phys. Chem. Lett., 8, https://doi.org/10.1021/acs.jpclett.7b02105, 2017.

Gately, C. K. and Hutyra, L. R.: Large Uncertainties in Urban-Scale Carbon Emissions, J. Geophys. Res. Atmos., 122, 11,242-11,260, https://doi.org/10.1002/2017JD027359, 2017.

Genoud, G., Lehmuskoski, J., Bell, S., Palonen, V., Oinonen, M., Koskinen-Soivi, M. L., and

375    Reinikainen, M.: Laser Spectroscopy for Monitoring of Radiocarbon in Atmospheric Samples, Anal. Chem., 91, https://doi.org/10.1021/acs.analchem.9b02496, 2019.

Gourdji, S. M., Karion, A., Lopez-Coto, I., Ghosh, S., Mueller, K. L., Zhou, Y., Williams, C. A.,

Baker, I. T., Haynes, K. D., and Whetstone, J. R.: A Modified Vegetation Photosynthesis and Respiration Model (VPRM) for the Eastern USA and Canada, Evaluated With Comparison to

380    Atmospheric Observations and Other Biospheric Models, J. Geophys. Res. Biogeosciences, 127, https://doi.org/10.1029/2021JG006290, 2022.

Graven, H. D., Stephens, B. B., Guilderson, T. P., Campos, T. L., Schimel, D. S., Campbell, J. E., and Keeling, R. F.: Vertical profiles of biospheric and fossil fuel-derived $CO_2$ and fossil fuel $CO_2$: CO ratios from airborne measurements of Δ14C, $CO_2$ and CO above Colorado, USA,

385    Tellus, Ser. B Chem. Phys. Meteorol., 61, https://doi.org/10.1111/j.1600-0889.2009.00421.x, 2009.

Gurney, K. R., Patarasuk, R., Liang, J., Song, Y., O&apos;Keeffe, D., Rao, P., Whetstone, J. R., Duren, R. M., Eldering, A., and Miller, C. E.: The Hestia Fossil Fuel $CO_2$ Emissions Data Product for the Los Angeles Megacity (Hestia-LA), Earth Syst. Sci. Data, 11, 1309–1335,

390    https://doi.org/10.5194/essd-2018-162, 2019.

Hardiman, B. S., Wang, J. A., Hutyra, L. R., Gately, C. K., Getson, J. M., and Friedl, M. A.: Accounting for urban biogenic fluxes in regional carbon budgets, Sci. Total Environ., 592, 366–372, https://doi.org/10.1016/j.scitotenv.2017.03.028, 2017.

He, L., Zeng, Z., Pongetti, T. J., Wong, C., Liang, J., Gurney, K. R., Newman, S., Yadav, V.,

395    Verhulst, K. R., Miller, C. E., Duren, R., Frankenberg, C., Wennberg, P. O., Shia, R., Yung, Y. L., and Sander, S. P.: Atmospheric Methane Emissions Correlate With Natural Gas Consumption From Residential and Commercial Sectors in Los Angeles, Geophys. Res. Lett., 46, 8563–8571, https://doi.org/10.1029/2019gl083400, 2019.

Heimburger, A., Harvey, R., Shepson, P. B., Stirm, B. H., Gore, C., Turnbull, J. C., Cambaliza,

400    M. O. L., Salmon, O. E., Kerlo, A.-E. M., Lavoie, T. N., Davis, K. J., Lauvaux, T., Karion, A., Sweeney, C., Brewer, W. A., Hardesty, R. M., and Gurney, K. R.: Assessing the optimized precision of the aircraft mass balance method for measurement of urban greenhouse gas emission rates through averaging, Elem Sci Anth, 5, 26, https://doi.org/10.1525/elementa.134, 2017.

Lauvaux, T., Miles, N. L., Deng, A., Richardson, S. J., Cambaliza, M. O., Davis, K. J., Gaudet,

405    B., Gurney, K. R., Huang, J., O'Keefe, D., Song, Y., Karion, A., Oda, T., Patarasuk, R., Razlivanov, I., Sarmiento, D., Shepson, P., Sweeney, C., Turnbull, J. C., and Wu, K.: High-resolution atmospheric inversion of urban $CO_2$ emissions during the dormant season of the Indianapolis flux experiment (INFLUX), J. Geophys. Res., 121, 5213–5236,

https://doi.org/10.1002/2015JD024473, 2016.

410    Lauvaux, T., Gurney, K. R., Miles, N. L., Davis, K. J., Richardson, S. J., Deng, A., Nathan, B. J., Oda, T., Wang, J. A., Hutyra, L., and Turnbull, J. C.: Policy-relevant assessment of urban CO2emissions, Environ. Sci. Technol., 54, 10237–10245, https://doi.org/10.1021/acs.est.0c00343, 2020.

Lehman, S. J., Miller, J. B., Wolak, C., Southon, J., Tans, P. P., Montzka, S. A., Sweeney, C.,

415    Andrews, A., LaFranchi, B., Guilderson, T. P., and Turnbull, J. C.: Allocation of Terrestrial Carbon Sources Using 14 CO 2 : Methods, Measurement, and Modeling, Radiocarbon, 55, https://doi.org/10.1017/s0033822200048414, 2013.

Levin, I. and Karstens, U.: Inferring high-resolution fossil fuel CO2 records at continental sites from combined 14CO2 and CO observations, Tellus, Ser. B Chem. Phys. Meteorol., 59, 245–

420    250, https://doi.org/10.1111/j.1600-0889.2006.00244.x, 2007.

Lopez, M., Schmidt, M., Delmotte, M., Colomb, A., Gros, V., Janssen, C., Lehman, S. J., Mondelain, D., Perrussel, O., Ramonet, M., Xueref-Remy, I., and Bousquet, P.: CO, NOx and 13CO2 as tracers for fossil fuel CO2: Results from a pilot study in Paris during winter 2010, Atmos. Chem. Phys., 13, 7343–7358, https://doi.org/10.5194/acp-13-7343-2013, 2013.

425    Mays, K. L., Shepson, P. B., Stirm, B. H., Karion, A., Sweeney, C., and Gurney, K. R.: Aircraft-based measurements of the carbon footprint of Indianapolis, Environ. Sci. Technol., 43, 7816–7823, https://doi.org/10.1021/es901326b, 2009.

McCartt, A. D. and Jiang, J.: Room-Temperature Optical Detection of 14CO2below the Natural Abundance with Two-Color Cavity Ring-Down Spectroscopy, ACS Sensors, 7,

430    https://doi.org/10.1021/acssensors.2c01253, 2022.

Mcdonald, B. C., McBride, Z. C., Martin, E. W., and Harley, R. A.: High-resolution mapping of motor vehicle carbon dioxide emissions, J. Geophys. Res. Atmos., 5283–5298, https://doi.org/10.1002/2013JD021219.Received, 2014.

Miller, J. B., Lehman, S. J., Montzka, S. A., Sweeney, C., Miller, B. R., Karion, A., Wolak, C.,

435    Dlugokencky, E. J., Southon, J., Turnbull, J. C., and Tans, P. P.: Linking emissions of fossil fuel CO2 and other anthropogenic trace gases using atmospheric 14CO2, J. Geophys. Res. Atmos., 117, https://doi.org/10.1029/2011JD017048, 2012.

Miller, J. B., Lehman, S. J., Verhulst, K. R., Miller, C. E., Duren, R. M., Yadav, V., Newman, S., and Sloop, C. D.: Large and seasonally varying biospheric CO2 fluxes in the Los Angeles

440    megacity revealed by atmospheric radiocarbon, Proc. Natl. Acad. Sci. U. S. A., 117, 26681–
26687, https://doi.org/10.1073/pnas.2005253117, 2020.

Newman, S. and Jeong, S.: Diurnal tracking of anthropogenic CO2 emissions in the Los Angeles
basin megacity during spring 2010, Atmos. Chem. Phys., 4359–4372,
https://doi.org/10.5194/acp-13-4359-2013, 2013.

445    Newman, S., Xu, X., Affek, H. P., Stolper, E., and Epstein, S.: Changes in mixing ratio and
isotopic composition of CO2 in urban air from the Los Angeles basin, California, between 1972
and 2003, J. Geophys. Res. Atmos., 113, 1–15, https://doi.org/10.1029/2008JD009999, 2008.

Newman, S., Xu, X., Gurney, K. R., Hsu, Y. K., Li, K. F., Jiang, X., Keeling, R. F., Feng, S.,
O'Keefe, D., Patarasuk, R., Wong, K. W., Rao, P., Fischer, M. L., and Yung, Y. L.: Toward

450    consistency between trends in bottom-up CO2 emissions and top-down atmospheric
measurements in the Los Angeles megacity, Atmos. Chem. Phys., 16, 3843–3863,
https://doi.org/10.5194/acp-16-3843-2016, 2016.

Sargent, M., Barrera, Y., Nehrkorn, T., Hutyra, L. R., Gately, C. K., Jones, T., McKain, K.,
Sweeney, C., Hegarty, J., Hardiman, B., and Wofsy, S. C.: Anthropogenic and biogenic CO2

455    fluxes in the Boston urban region, Proc. Natl. Acad. Sci., 115, 7491–7496,
https://doi.org/10.1073/pnas.1803715115, 2018.

Staufer, J., Broquet, G., Bréon, F. M., Puygrenier, V., Chevallier, F., Xueref-remy, I.,
Dieudonné, E., Lopez, M., Schmidt, M., Ramonet, M., Perrussel, O., Lac, C., Wu, L., and Ciais,
P.: The first 1-year-long estimate of the Paris region fossil fuel CO2 emissions based on

460    atmospheric inversion, Atmos. Chem. Phys., 14703–14726, https://doi.org/10.5194/acp-16-
14703-2016, 2016.

Stuiver, M. and Polach, H. A.: Discussion: Reporting of 14C Data, Radiocarbon, 19, 355–363,
1977.

Super, I., Dellaert, S. N. C., Visschedijk, A. J. H., and Van Der Gon, H. A. C. D.: Uncertainty

465    analysis of a European high-resolution emission inventory of CO2 and CO to support inverse
modelling and network design, Atmos. Chem. Phys., 20, https://doi.org/10.5194/acp-20-1795-
2020, 2020.

Sweeney, C., Karion, A., Wolter, S., Newberger, T., Guenther, D., Higgs, J. A., Andrews, A. E.,
Lang, P. M., Neff, D., Dlugokencky, E., Miller, J. B., Montzka, S. A., Miller, B. R., Masarie, K.

470    A., Biraud, S. C., Novelli, P. C., Crotwell, M., Crotwell, A. M., Thoning, K., and Tans, P. P.:

Seasonal climatology of CO2 across North America from aircraft measurements in the NOAA/ESRL Global Greenhouse Gas Reference Network, J. Geophys. Res. Atmos., 5155–5190, https://doi.org/10.1002/2014JD022591.Received, 2015.

Turnbull, J. C., Karion, A., Fischer, M. L., Faloona, I., Guilderson, T., Lehman, S. J., and Miller, B. R.: Assessment of fossil fuel carbon dioxide and other anthropogenic trace gas emissions from airborne measurements over Sacramento, California in spring 2009, Atmos. Chem. Phys., 705–721, https://doi.org/10.5194/acp-11-705-2011, 2011.

Turnbull, J. C., Sweeney, C., Karion, A., Newberger, T., Lehman, S. J., Tans, P. P., Davis, K. J., Lauvaux, T., Miles, N. L., Richardson, S. J., Cambaliza, M. O., Shepson, P. B., Gurney, K. R., Patarasuk, R., and Razlivanov, I.: Toward quantification and source sector identification of fossil fuel CO2 emissions from an urban area: Results from the INFLUX experiment, J. Geophys. Res., 120, 292–312, https://doi.org/10.1002/2014JD022555, 2015.

Turnbull, J. C., Karion, A., Davis, K. J., Lauvaux, T., Miles, N. L., Richardson, S. J., Sweeney, C., McKain, K., Lehman, S. J., Gurney, K. R., Patarasuk, R., Liang, J., Shepson, P. B., Heimburger, A., Harvey, R., and Whetstone, J.: Synthesis of Urban CO2 Emission Estimates from Multiple Methods from the Indianapolis Flux Project (INFLUX), Environ. Sci. Technol., 53, 287–295, https://doi.org/10.1021/acs.est.8b05552, 2019.

Turnbull, J. C., DeCola, P., Mueller, K., and Vogel, F.: IG3IS Urban Greenhouse Gas Emission Observation and Monitoring Best Research Practices, World Meteorological Organization, 2022.

Turner, A. J., Kim, J., Fitzmaurice, H., Newman, C., Worthington, K., Chan, K., Wooldridge, P., Köhler, P., Frankenberg, C., and Cohen, R. C.: Observed impacts of COVID-19 on urban CO2 emissions, Geophys. Res. Lett., 2–10, 2020.

Vardag, S. N., Gerbig, C., Janssens-Maenhout, G., and Levin, I.: Estimation of continuous anthropogenic CO2: Model-based evaluation of CO2, CO, $\delta 13C(CO2)$ and $\Delta 14C(CO2)$ tracer methods, Atmos. Chem. Phys., 15, 12705–12729, https://doi.org/10.5194/acp-15-12705-2015, 2015.

Vaughn, B. H., Miller, J. B., Ferretti, D. F., and White, J. W. C.: Stable isotope measurements of atmospheric CO2 and CH4, in: Handbook of Stable Isotope Analytical Techniques, https://doi.org/10.1016/B978-044451114-0/50016-8, 2004.

Vimont, I. J., Turnbull, J. C., Petrenko, V. V., Place, P. F., Sweeney, C., Miles, N., Richardson, S., Vaughn, B. H., and White, J. W. C.: An improved estimate for the $\delta c$ and $\delta c$ signatures of

carbon monoxide produced from atmospheric oxidation of volatile organic compounds, Atmos. Chem. Phys., 19, 8547–8562, https://doi.org/10.5194/acp-19-8547-2019, 2019.

Vogel, F. R., Hammer, S., Steinhof, A., Kromer, B., and Levin, I.: Implication of weekly and diurnal 14C calibration on hourly estimates of CO-based fossil fuel $CO_2$ at a moderately polluted site in southwestern Germany, Tellus, Ser. B Chem. Phys. Meteorol., 62, 512–520, https://doi.org/10.1111/j.1600-0889.2010.00477.x, 2010.

Vogel, F. R., Frey, M., Staufer, J., Hase, F., Broquet, G., and Xueref-remy, I.: $XCO_2$ in an emission hot-spot region : the COCCON Paris campaign 2015, Atmos. Chem. Phys., 19, 3271–3285, 2019.

Winbourne, J. B., Smith, I. A., Stoynova, H., Kohler, C., Gately, C. K., Logan, B. A., Reblin, J., Reinmann, A., Allen, D. W., and Hutyra, L. R.: Quantification of Urban Forest and Grassland Carbon Fluxes Using Field Measurements and a Satellite-Based Model in Washington DC/Baltimore Area, J. Geophys. Res. Biogeosciences, 127, https://doi.org/10.1029/2021JG006568, 2022.

Wu, D., Lin, J. C., Duarte, H. F., Yadav, V., Parazoo, N. C., Oda, T., and Kort, E. A.: A model for urban biogenic $CO_2$ fluxes: Solar-Induced Fluorescence for Modeling Urban biogenic Fluxes (SMUrF v1), Geosci. Model Dev., 14, https://doi.org/10.5194/gmd-14-3633-2021, 2021.
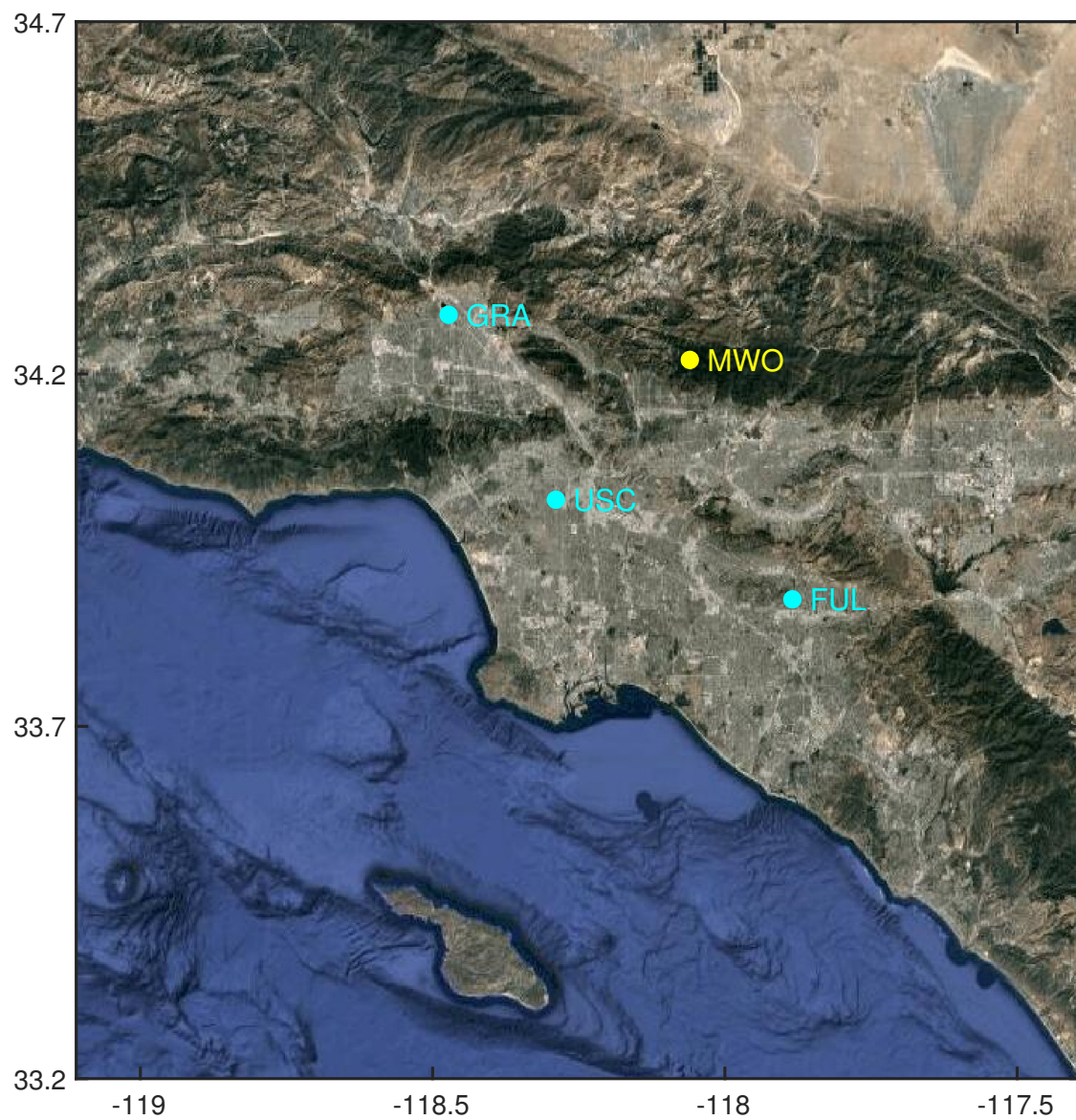
**Figure 1.** Map of the greater Los Angeles region. The three Los Angeles Megacity Carbon Project sites are marked in cyan and the Mount Wilson Observatory used to define background values are marked in yellow. Map data © Google Maps 2022.
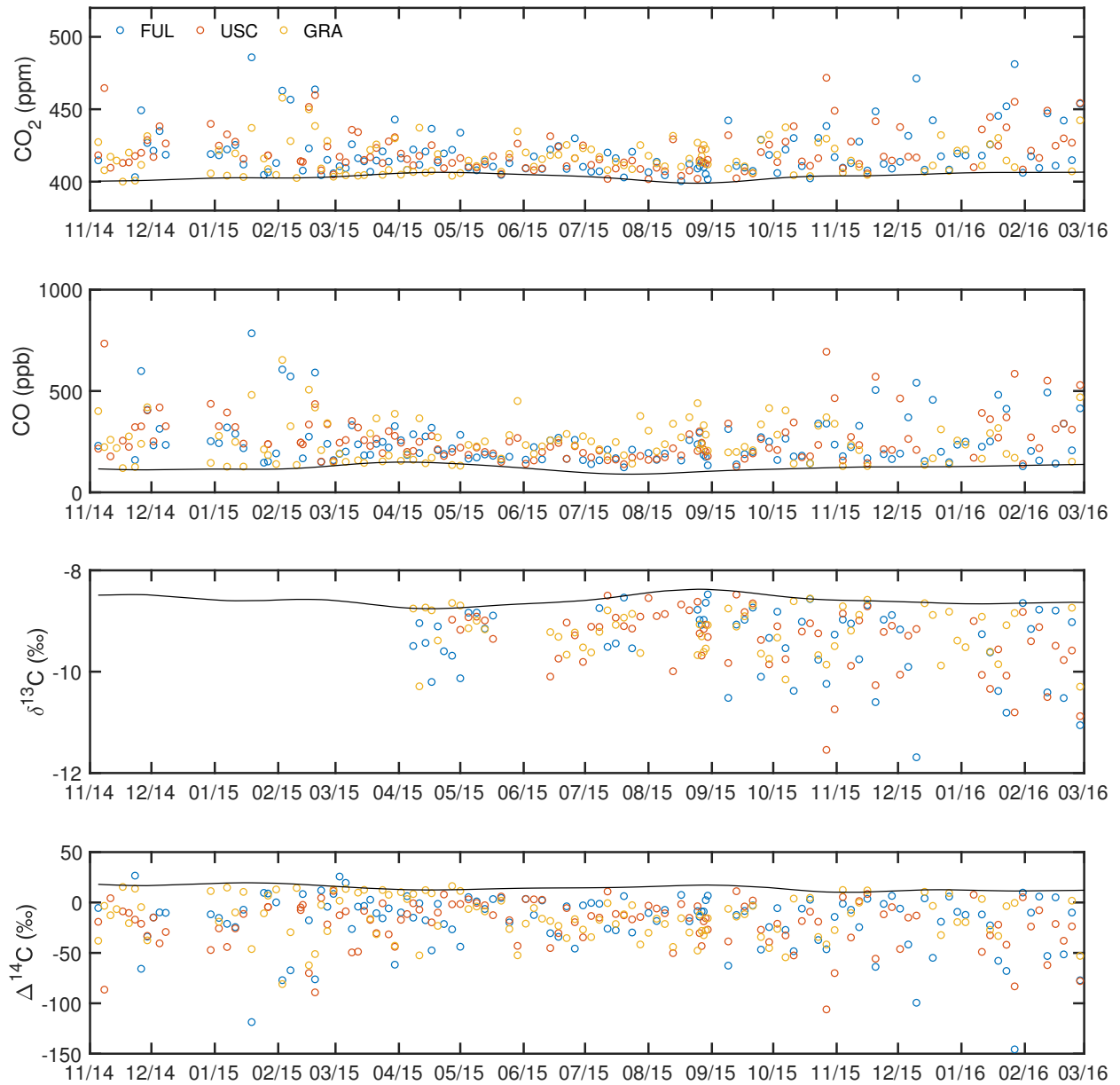
**Figure 2.** Timeseries of $CO_2$, CO, $\delta^{13}C$, and $\Delta^{14}C$. Black line represents background values. Dates are labeled in month/year.
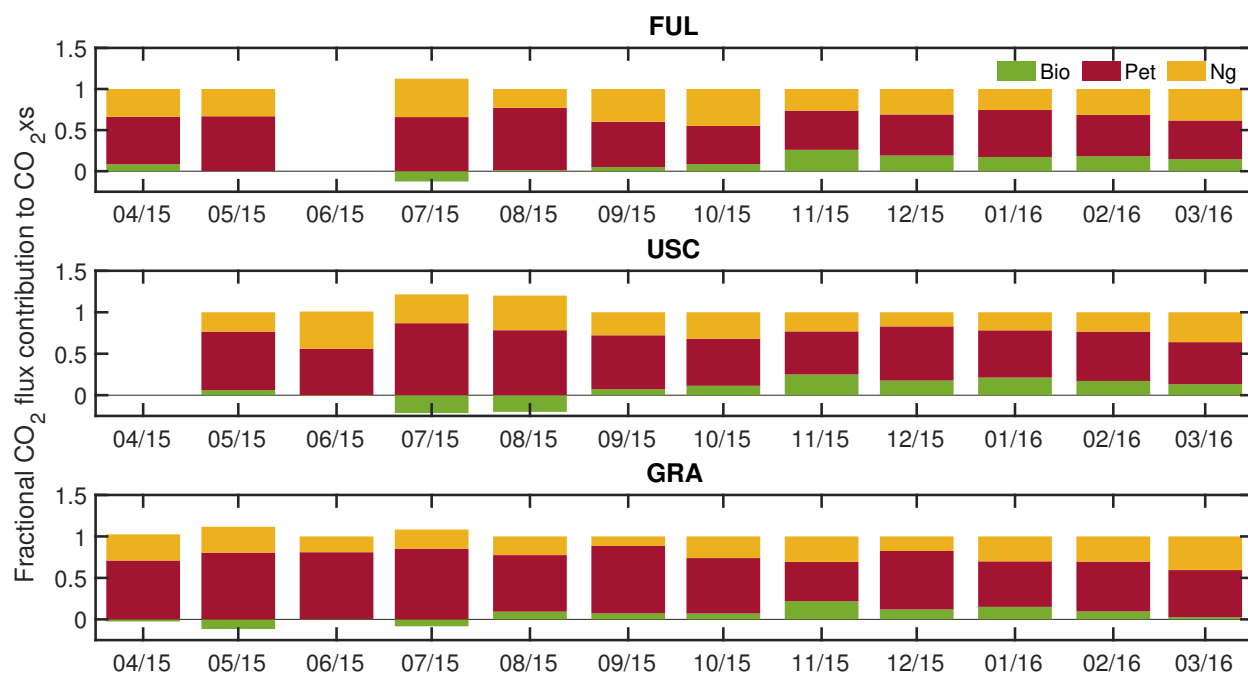
**Figure 3.** Monthly mean fractional contributions (f) of biosphere (green), petroleum (red), and natural gas (yellow) to $CO_2$xs at each site, as determined from $\Delta^{14}C$ and $\delta^{13}C$ observations (Section 2.2). The sum of the fractions is one in each month. Dates are labeled in month/year.
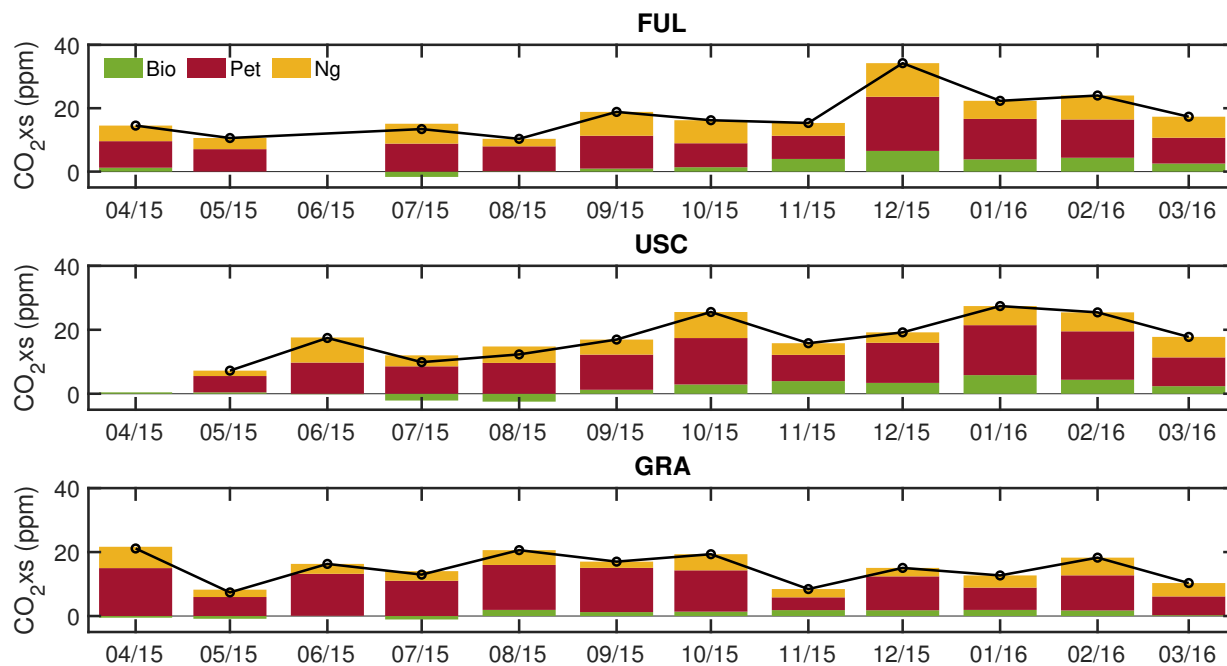
**Figure 4.** Monthly mean $CO_2$xs partitioned into biosphere (green), petroleum (red), and natural gas (yellow) signals, as determined from $\Delta^{14}C$ and $\delta^{13}C$ observations, at each site. The black marker indicates $CO_2$xs. Dates are labeled in month/year.
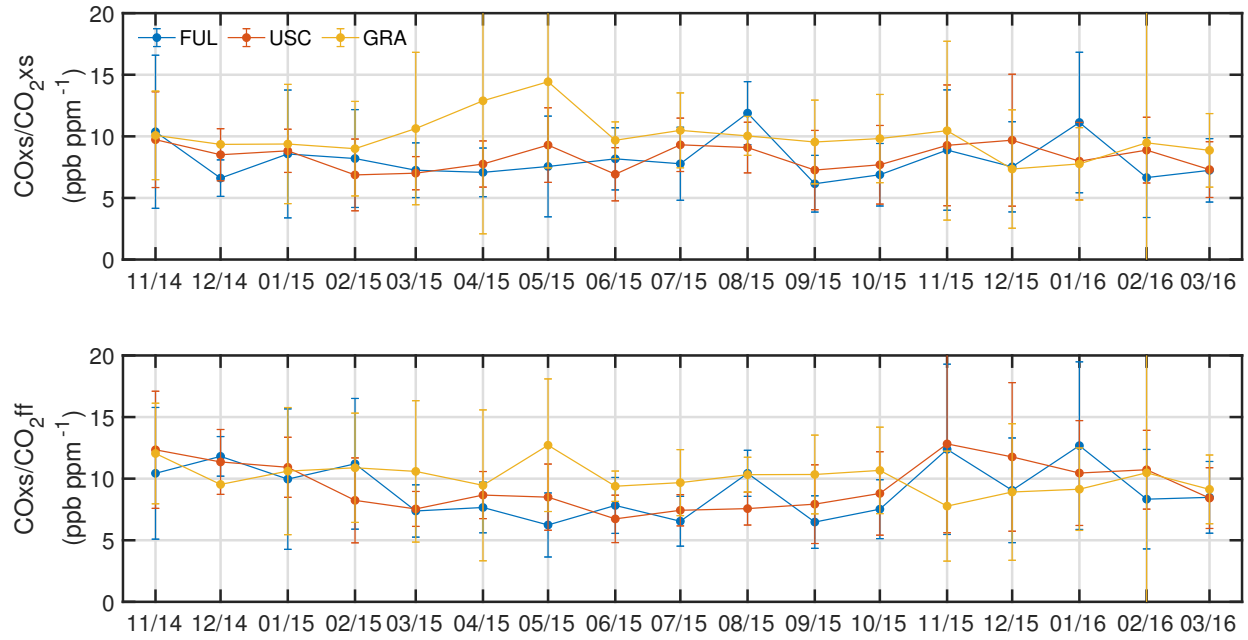
**Figure 5.** Monthly variations in COxs/$CO_2$xs (Rsrc) and COxs/$CO_2$ff (Rff) at each site. COxs/$CO_2$ff is calculated using $^{14}C$ observations. Dates are labeled in month/year.
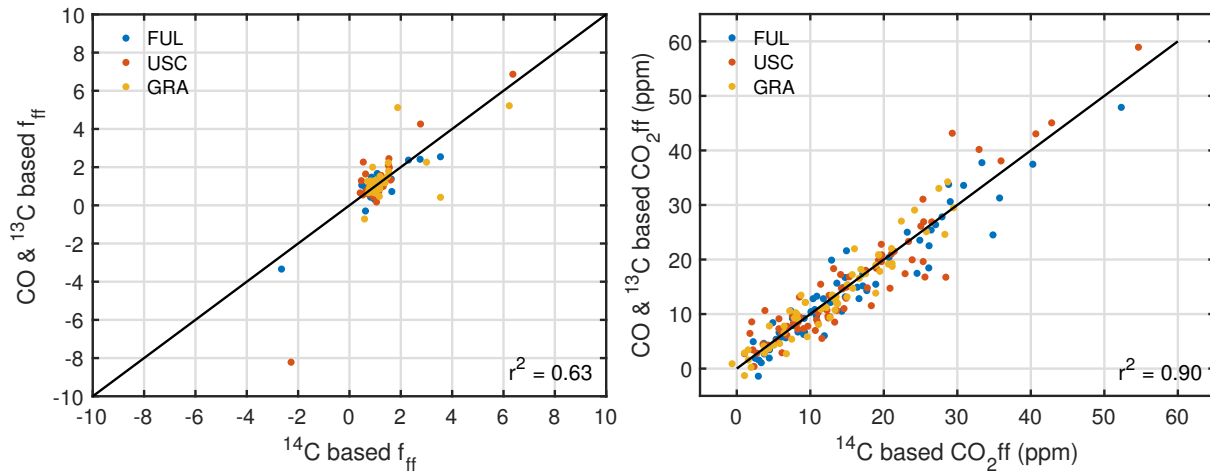
565

**Figure 6.** Comparison of $f_{ff}$ and $f'_{ff}$ (left) and $C_{ff}$ and $C'_{ff}$ (right). Black lines represent 1:1 relationships and different colors indicate different sites.
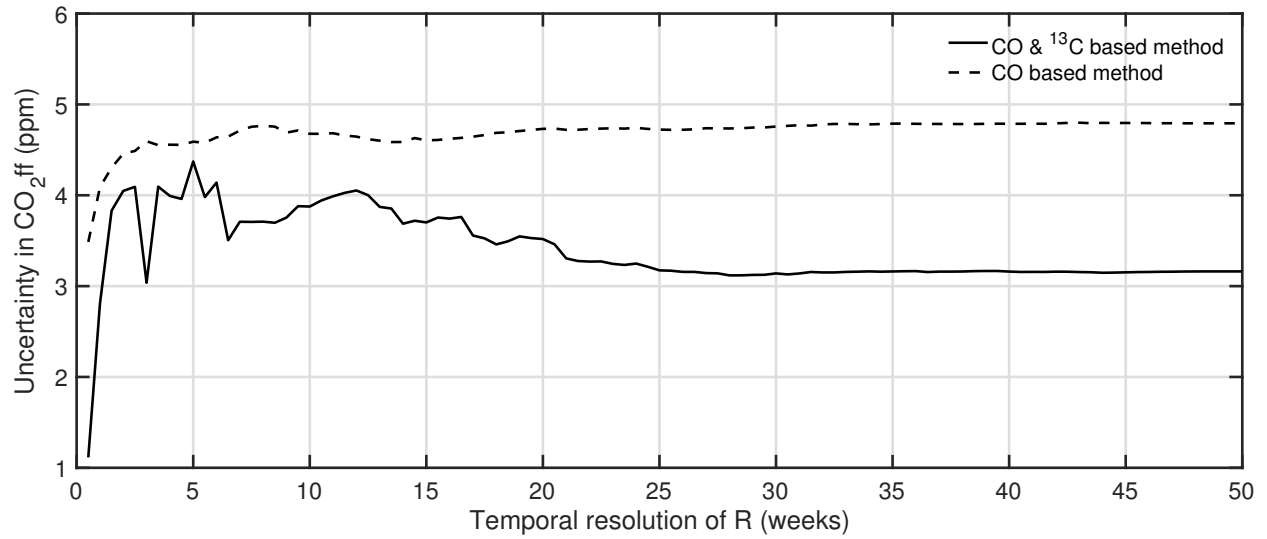
570

**Figure 7.** Uncertainty in $C'_{ff}$ for varying temporal resolution of $R$ (N weeks). $R$ is determined for each data point solving Eq. 7 using CO, $^{13}CO_2$ and $^{14}CO_2$ observations within a moving window of 2N weeks. For CO-based method, $R_{ff}$ is smoothed using a 2N weeks moving window.

575

**Table 1.** Bottom-up $CO_2$ emission, CO emission, and R ($CO/CO_2$ ratio) estimates for each source sector and fuel type for LA basin based on the Vulcan 3.0 and the U.S. Environmental Protection Agency (EPA) National Emission Inventory for 2011 (NEI 2011) product. NEI 2011 is scaled by the emissions with fuel consumption dataset from the U.S. Energy Information Administration (EIA) State Energy Data System (SEDS) to estimate 2015 CO emissions.

| | ------------Petroleum-------------- | | | -----------Natural Gas---------- | | |
| | $CO_2$ (MtC) | CO (MtC) | R = CO/CO$_2$ (ppb ppm$^{-1}$) | $CO_2$ (MtC) | CO (MtC) | R = CO/CO$_2$ (ppb ppm$^{-1}$) |
|---|---|---|---|---|---|---|
| Residential | 0.06 | <0.001 | 0.03 | 2.79 | 0.001 | 0.52 |
| Commercial | 0.67 | <0.001 | 0.15 | 1.79 | 0.002 | 1.09 |
| Industrial | 9.79 | <0.001 | 0.02 | 1.59 | 0.002 | 1.28 |
| Electricity Production | 0.37 | <0.001 | 0.02 | 5.08 | 0.002 | 0.32 |
| On-road | 20.97 | 0.296 | 13.62 | 0 | 0 | |
| Non-road | 1.45 | 0.139 | 96.05 | 0.19 | 0.012 | 65.32 |
| Airport | 0.89 | 0.008 | 9.27 | 0 | 0 | |
| Rail | 0.47 | 0.002 | 5.12 | 0 | 0 | |
| CMV | 0.48 | <0.001 | 1.40 | 0 | 0 | |
| **Total** | **35.16** | **0.437** | **12.42** | **11.44** | **0.019** | **1.68** |

585    **Table 2.** CO/CO$_2$ ratios ($R$) and $\delta^{13}$C signatures used to determine relative contribution of biogenic, petroleum and natural gas sources.

|  | Biosphere | Petroleum | Natural Gas |
|---|---|---|---|
| Bottom-up approach $R$ (ppb ppm$^{-1}$)[a] |  | 12.4 | 1.7 |
| Top-down approach $R$ (ppb ppm$^{-1}$)[b] | $1.8 \pm 0.8$ | $12.2 \pm 0.6$ | $2.3 \pm 1.2$ |
| $\delta^{13}$C (‰)[c] | $-26.6 \pm 0.5$ | $-25.5 \pm 0.5$ | $-40.2 \pm 0.5$ |

590    [a]$R$ calculated from Table 1. These values are not used for CO$_2$xs partitioning and are for reference only.
[b]$R$ calculated from CO, $\delta^{13}$CO$_2$ and $\Delta^{14}$CO$_2$ flask observations. These values are used in this study.
[c]$\delta^{13}$C from previous studies (Bakwin et al., 1998a; Newman et al., 2008)